



Results of 23 yr of Pulsar Timing of PSR J1453-6413

Wei Li^{1,2} , Shi-Jun Dang^{1,2,3} , Jian-Ping Yuan⁴, Lin Li⁵, Wei-Hua Wang⁶, Lun-Hua Shang^{1,2}, Na Wang⁴, Qing-Ying Li^{1,2}, Ji-Guang Lu⁷, Fei-Fei Kou⁴, Shuang-Qiang Wang⁴, Shuo Xiao^{1,2}, Qi-Jun Zhi^{1,2}, Yu-Lan Liu^{3,7,8}, Ru-Shuang Zhao^{1,2}, Ai-Jun Dong^{1,2}, Bin Zhang^{1,2}, Zi-Yi You^{1,2}, Yan-Qing Cai^{1,2}, Ya-Qin Yang¹, Ying-Ying Ren^{1,2}, Yu-Jia Liu^{1,2}, and Heng Xu^{1,2}

¹School of Physics and Electronic Science, Guizhou Normal University, Guiyang 550001, China; dangsj@gznu.edu.cn, lhshang@gznu.edu.cn

²Guizhou Provincial Key Laboratory of Radio Astronomy and Data Processing, Guizhou Normal University, Guiyang 550001, China; qjzhi@gznu.edu.cn

³Guizhou Radio Astronomy Observatory, Guizhou University, Guiyang 550025, China

⁴Xinjiang Astronomical Observatory, Chinese Academy of Sciences, Urumqi 830011, China

⁵School of Physics Science and Technology, Xinjiang University, Urumqi 830046, China

⁶College of Mathematics and Physics, Wenzhou University, Wenzhou 325035, China

⁷National Astronomical Observatories, Chinese Academy of Sciences, Beijing 100101, China

⁸CAS Key Laboratory of FAST, National Astronomical Observatories, Chinese Academy of Sciences, Beijing 100101, China

Received 2023 June 19; accepted 2023 July 5; published 2023 September 27

Abstract

In this paper, we presented the 23.3 yr of pulsar timing results of PSR J1456–6413 based on the observations of Parkes 64 m radio telescope. We detected two new glitches at MJD 57093(3) and 59060(12) and confirmed its first glitch at MJD 54554(10). The relative sizes ($\Delta\nu/\nu$) of these two new glitches are 0.9×10^{-9} and 1.16×10^{-9} , respectively. Using the “Cholesky” timing analysis method, we have determined its position, proper motion, and two-dimensional transverse velocities from the data segments before and after the second glitch, respectively. Furthermore, we detected exponential recovery behavior after the first glitch, with a recovery timescale of approximately 200 days and a corresponding exponential recovery factor Q of approximately 0.15(2), while no exponential recovery was detected for the other two glitches. More interestingly, we found that the leading component of the integral pulse profile after the second glitch became stronger, while the main component became weaker. Our results will expand the sample of pulsars with magnetosphere fluctuation triggered by the glitch event.

Key words: Stars – (stars): pulsars: individual (PSR J1453-6413) – stars: neutron

1. Introduction

Pulsars are rapidly rotating neutron stars with high magnetic fields. Due to the remarkable stability of pulsar rotation, they are considered the ideal clocks. Pulsar timing studies can be carried out with long-term observation records of the arrival time of pulsar pulses to the Earth, and comparison with theoretical models to obtain the arrival time residual, so as to study the physics involved. Pulsar timing can be used for obtaining its rotational and astrometric parameters, detecting the internal states of neutron stars, testing general relativity (Hobbs et al. 2004), detecting gravitational waves (Kramer et al. 2006), pulsar navigation (Deng et al. 2013) and pulsar clocks (Liu et al. 2023). However, long-term timing observations show that the spin frequency ν of some pulsars evolves irregularly. Timing noise and glitches are two main manifestations of this irregularity.

Timing noise, which is often presented as non-whiten and un-modeled timing residual, is a significant deviation of the pulsar rotation from the spin-down model indicating erratic fluctuation in the rotation of the pulsar. The phenomenon is classified as low-frequency noise or red noise and usually has time scales of months to years (Hobbs et al. 2010). The nature of timing noise is still unclear, but it has been attributed to

either fluctuation in the spin-down or magnetospheric torque (Cheng 1987a, 1987b), or variation of the coupling between the stellar crust and its superfluid core (Jones 1990). Timing noise has also been proposed that the macroscopic turbulence in the neutron star’s core superfluid can lead to instability in the spin-down processes (Melatos & Link 2014).

A glitch appears as a sudden increase in the pulsar spin frequency. Glitches usually can be divided into large glitches $\sim 10^{-5}$ and small glitches $\sim 10^{-10}$ according to the value of $\Delta\nu/\nu$. Generally, the evolution of ν of the post glitch tends to present exponential recovery, and the spin-down rate $|\dot{\nu}|$ will increase first and then decay to the level of the pre-glitch. The relaxation time of exponential recovery can vary greatly between pulsars and even after different glitches in the same pulsar (D’Alessandro 1996; Yuan et al. 2010a, 2010b; Espinoza et al. 2011; Yu et al. 2013; Dang et al. 2020).

Generally, the glitch is thought to originate inside a neutron star. Two main mechanisms have been proposed to explain this phenomenon. The first mechanism suggests that the crust earthquakes in neutron stars cause an increasing amount of strain to accumulate in the crust, leading to a sudden rearrangement of the moment of inertia (Ruderman 1991; Ruderman et al. 1998). But this hypothesis is weak in

Table 1
The Positions of PSR J1453–6413 in J2000 Equatorial Coordinates

RAJ (h:m:s)	DECJ (d:m:s)	POSEPOCH MJD	Data Range MJD	Reference
14:53:32.665(6)	–64:13:16.00(5)	55433	54220–58012	(Parthasarathy et al. 2019)
14:53:32.663(6)	–64:13:15.99(5)	55811	54566–57057	This Work
14:53:32.653(1)	–64:13:16.070(9)	58082	57129–59035	This Work

explaining large glitches. The second mechanism is the sudden transfer of the moment of inertia carried by the superfluid inside the neutron star to its crust, resulting in the observed sudden increase in spin frequency (Anderson & Itoh 1975; Ruderman 1976). This hypothesis successfully explains the post-glitch relaxation of PSR J1453–6413 and other pulsars. However, recent observations have shown that glitches in some pulsars are connected with the changes in their pulse profiles, such as PSRs J1119–6127, J2036+2740, J0738–4042, J0742–2822, J0835–4510, B2021+51 and B1822–09 (Weltevrede et al. 2011; Keith et al. 2013; Kou et al. 2018; Palfreyman et al. 2018; Dang et al. 2021; Liu et al. 2022; Zhou et al. 2023). This may imply that the pulsar glitches are related to their magnetosphere activity.

PSR J1453–6413 is a normal middle age pulsar with spin period $P \approx 0.179$ s (Parthasarathy et al. 2019), and the characteristic age $\tau_c \equiv -\frac{\nu}{(2\dot{\nu})} \approx 1.037$ Myr, distance $D \approx 2.8$ kpc. Only one glitch of this pulsar at MJD 54 552(4) was reported by the previous work, and the relative size of this glitch is $\Delta\nu/\nu \approx 2.99(18) \times 10^{-10}$ with the relative change of spin-down rate $\Delta\dot{\nu}/\dot{\nu} \approx 0.55(11) \times 10^{-3}$ (Yu et al. 2013).

In this paper, we have studied the timing behavior of PSR J1453–6413 using 23.3 yr of timing observations of the 64m Radio Telescope (Parkes) in Australia at the central frequency of 1369 MHz. We have found two new glitches in this pulsar and obtained the new proper motion and position using the ‘‘Cholesky’’ timing analysis method. In Section 2, we introduce the observation and data process. In Section 3, we report the results of the timing analysis. Discussion and conclusions follow in Sections 4 and 5.

2. Observation and Data Analyses

We analyzed timing observations of PSR J1453–6413 from 1998 July to 2021 October, which are publicly available to download from the Parkes pulsar data archive⁹ (Hobbs et al. 2011). The data before MJD 54303 has a center frequency of 1374 MHz and a bandwidth of 256 MHz. In addition, the Parkes Analog Filter Bank system (AFB) was used in the observation during this data segment. The data between MJD 54303 and 58686 have a center frequency of 1369 MHz and a bandwidth of 256 MHz, and the multi-beam receiver and the

Parkes Digital Filter Bank systems (PDFB1/2/3/4) have been used in the observations. Furthermore, the vast majority of data from MJD 58 430 to 59514 was observed with the ultrawide-bandwidth receiver. The time intervals of observation are usually 2–4 weeks/time, the sub-integration time of each observation is 30 s, and the total integration time is 2–15 minutes.

After obtaining the data, we used the software PSRCHIVE¹⁰ (Hotan et al. 2004) and the software packages TEMPO2¹¹ (Hobbs et al. 2006) for offline data processing. First, PSRCHIVE was used to remove radio frequency interference (RFI) and incoherent dispersion from data, and time, frequency, and polarization were summed to form an integral pulse profile. Second, we select the one with the highest signal-to-noise ratio (S/N) as the standard template and used command PAT in PSRCHIVE to cross-correlational all the average pulse profiles with the standard template to get time-of-arrival (ToA). In order to eliminate the influence of Earth’s motion, we transformed these ToAs to the solar system barycenter (SSB) using the solar ephemeris DE436 and TEMPO2 software packages, which can be regarded as an inertial reference frame. Finally, to obtain the high-precision timing solution, we employ the ‘‘Cholesky’’ timing analysis method to fit the red noise model, which can be achieved by the SPECTRALMODEL plugin of TEMPO2 software package. The detailed implementation steps of the SPECTRALMODEL plugin are seen (Dang et al. 2020). Offset between different observing systems was also included.

3. Results

3.1. Position and Proper Motion

Based on the above methods, we determined the position, proper motion, and transverse velocity of PSR J1453–6413. Table 1 lists the position of this pulsar, including the positions from the previous publication of the ATNF pulsar catalog¹² (Manchester et al. 2005) and the parameters obtained by this work. The first and second columns list the Right Ascension (R.A.) and decl. (decl.) in J2000 Equatorial Coordinates respectively. The third column lists the reference time for the

⁹ <https://data.csiro.au/dap/public/atnf/pulsarSearch.zul>

¹⁰ <http://psrchive.sourceforge.net/>

¹¹ <https://bitbucket.org/psrsoft/tempo2/>

¹² <http://www.atnf.csiro.au/research/pulsar/psrcat/>

Table 2
The Proper Motion of PSR J1453–6413

μ_α (mas yr ⁻¹)	μ_δ (mas yr ⁻¹)	Data Range MJD	Reference
-16.4(11)	-21.30(76)	54597–57057	(Bailes et al. 1990)
-14(32)	0(41)	54597–57057	This Work
-9(17)	-14(21)	57129–59035	This Work

position. The corresponding data range for each position is listed in the fourth column. The first line shows the results from the literature. The bottom two lines show the results from our timing analyses. Uncertainties in each parameter are in the last quoted digit and are 1σ (Tables 2, 4, and 5 are the same). Compared with the position precision given in the literature, the precision of decl. obtained by the data segment in 57129–59035 is higher.

Table 2 lists the proper motion obtained by our timing analysis and the literature. In our analysis, the parameters of proper motion before and after the second glitch are determined, respectively. The first and second columns list μ_α and μ_δ , which are projections of proper motion on R.A. and decl., respectively. The first line shows the result of previous analyses. The bottom two lines show the results of our timing analyses.

When analyzing the proper motion of PSR J1453–6413, we found that the proper motion of this pulsar changed before and after the second glitch. Due to the impact of this glitch, it was difficult to determine the proper motion in the whole data span. Therefore, we take the epoch of the second glitch as the boundary and get the proper motions of the pre and post-glitch data span, respectively. The values of proper motion in R.A. and decl. of the pre-glitch are $\mu_\alpha = -14(32)\text{mas yr}^{-1}$ and $\mu_\delta = 0(41)\text{mas yr}^{-1}$. The values of proper motion in RAJ and DECJ for the post-glitch data span are $\mu_\alpha = -9(17)\text{mas yr}^{-1}$ and $\mu_\delta = -14(21)\text{mas yr}^{-1}$. Obviously, our results are well consistent with the literature in the error range.

3.2. Velocity

In general, if the proper motion and distance of a pulsar are known, its 2D transverse velocity can be given by $V_T = 4.74 \mu_{\text{tot}} D \text{ km s}^{-1}$, where $\mu_{\text{tot}} = \sqrt{\mu_\alpha^2 + \mu_\delta^2}$ is the total proper motion in mas yr^{-1} , D is the distance of the pulsar in kpc. The uncertainties of the pulsar velocities can be calculated from the standard error transfer formula. The distance $D = 2.8 \text{ kpc}$ was obtained by measuring the absorption line of HI, and the distance $D^Y = 1.432 \text{ kpc}$ was estimated using the YMW16 Galactic free-electron density model (Yao et al. 2017). In addition, the uncertainties of the distances D are 40% (Yao et al. 2017). We obtained the 2D transverse velocities V_T

Table 3
The 2D Transverse Velocities of PSR J1453–6413

D (kpc)	V_T (km s ⁻¹)	D^Y (kpc)	V_T^Y (km s ⁻¹)	Data Range MJD	Reference
2.2	238	54597–57057	(Bailes et al. 1990)
2.8(11)	186(431)	1.4(6)	95(221)	54597–57057	This Work
2.8(11)	221(278)	1.4(6)	113(143)	57129–59035	This Work

Table 4
The Rotation Parameters of PSR J1453–6413

ν (s ⁻¹)	$\dot{\nu}$ 10^{-14} s^{-2}	Epoch (MJD)	Data Range (MJD)
5.57144894977(4)	-8.52013(3)	54246	50947–54549
5.571437431605(6)	-8.51892(2)	55811	54565–57057
5.571420718074(1)	-8.518586(6)	58082	57129–59035
5.57141176670(3)	-8.5203(7)	59299	59084–59514

of PSR J1453–6413 for the pre and post-glitch data span (see: Table 3).

Table 3 lists the 2D transverse velocity from the previous literature and our results, respectively. The distances are given in the first and third columns, the 2D transverse velocities are given in the second and fourth columns, and data ranges are given in the fifth column. The last column lists the reference. The distance and velocities with superscript “Y” represent those obtained using the YMW16 model. The first line shows the results of the literature. The bottom two lines show the results of our timing analyses. Obviously, these velocity values are also consistent within the range of the error bar.

3.3. Glitch

Excepting the first glitch at MJD 54548(10), two new glitches were detected in PSR J1453–6413 at MJD 57093(3) and 59060(12). We divided the data span into four segments according to the epoch of these three glitches and then obtained the corresponding rotation parameters (ν and $\dot{\nu}$). Uncertainties for the rotation parameters are 1σ from TEMPO2 (see: table 4). In addition, we adapt the midpoint of the last observed epoch (T1) before the glitch and the first observed epoch after the glitch as the glitch epoch, and define (T2-T1)/4 as the 1σ uncertainty of the glitch epoch (Espinoza et al. 2011). Table 5 shows ν , $\dot{\nu}$, and their reference time and the corresponding data range from left to right, respectively.

Figure 1 shows the evolution of ν and $\dot{\nu}$ for the three glitches. Obviously, there is a significant recovery process after the first and second glitches, but due to the limited amount of data points, we cannot see its recovery behavior after the third

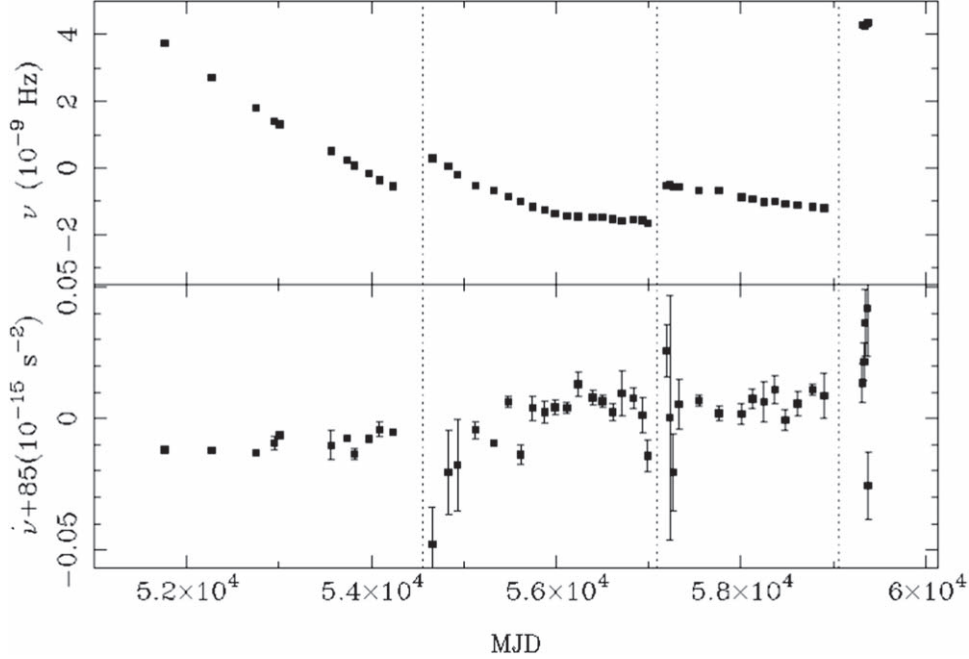


Figure 1. The glitches of PSR J1453–6413. The upper panel is ν with a gradient removed, and the unit is Hz. The bottom panel is $\dot{\nu}$ with the mean post-glitch values removed, and the unit is s^{-2} . Each vertical dashed line presents for the glitch epoch. The horizontal axis of each panel is time (MJD).

Table 5
The Glitch Parameters of PSR J1453–6413

Gl.No.	Epoch (MJD)	$\Delta\nu$ (10^{-9})	$\Delta\dot{\nu}$ (10^{-15})	$\Delta\nu/\nu$ (10^{-9})	$\Delta\dot{\nu}/\dot{\nu}$ (10^{-3})	τ_d (Day)	Q
1	54554(10)	1.1(2)	−0.03(1)	1.9(4)	0.3(2)	200	0.15(2)
2	57093(3)	1.16(1)	−0.0030(3)	0.208(3)	0.035(3)
3	59060(12)	6.57(4)	−0.042(2)	1.180(7)	0.50(2)

glitch. In order to quantitatively describe the size of the glitch and the rotation evolution behavior before and after these glitches, the glitch parameters are determined by the TEMPO2. The details are as follows:

In the data processing of the glitch of a pulsar, we pay more attention to its rotational phase, which can be expressed by Taylor series expansion,

$$\phi(t) = \phi(t_0) + \nu(t - t_0) + \frac{\dot{\nu}}{2}(t - t_0)^2 + \frac{\ddot{\nu}}{6}(t - t_0)^3 + \dots, \quad (1)$$

where $\phi(t_0)$ is the pulse phase at the barycentric reference time t_0 . Here, ν , $\dot{\nu}$, and $\ddot{\nu}$ represent the spin frequency, the first derivative of frequency (the spin-down rate), and the second derivative of frequency respectively. The glitch is identified by a sudden discontinuity in the timing residuals relative to a pre-glitch solution. These pulse phase jumps can usually be

described as the increase in the ν and $\dot{\nu}$ as follows (Edwards et al. 2006):

$$\phi_g = \Delta\phi + \Delta\nu_p(t - t_g) + \frac{1}{2}\Delta\dot{\nu}_p(t - t_g)^2 \times [1 - e^{-(t-t_g)/\tau_d}]\Delta\nu_d\tau_d, \quad (2)$$

where t_g is the time of glitch, $\Delta\phi$ is the increment of pulse phase in the data before and after the glitch. Glitch is characterized by a permanent increase of spin frequency $\Delta\nu_p$, a permanent increase of the first derivative of spin frequency $\Delta\dot{\nu}_p$ and a transient frequency increment $\Delta\nu_d$, and the increment decays exponentially on the timescale τ_d . Then, increments on the spin frequency and spin-down rate are described by $\Delta\nu_g = \Delta\nu_p + \Delta\nu_d$ and $\Delta\dot{\nu}_g = \Delta\dot{\nu}_p - \frac{\Delta\nu_d}{\tau_d}$. The exponential recovery factor is defined as $Q \equiv \Delta\nu_d/\Delta\nu_g$. The glitches parameters of PSR J1453–6413 are given in Table 5. The errors are derived from the standard error transfer formula.

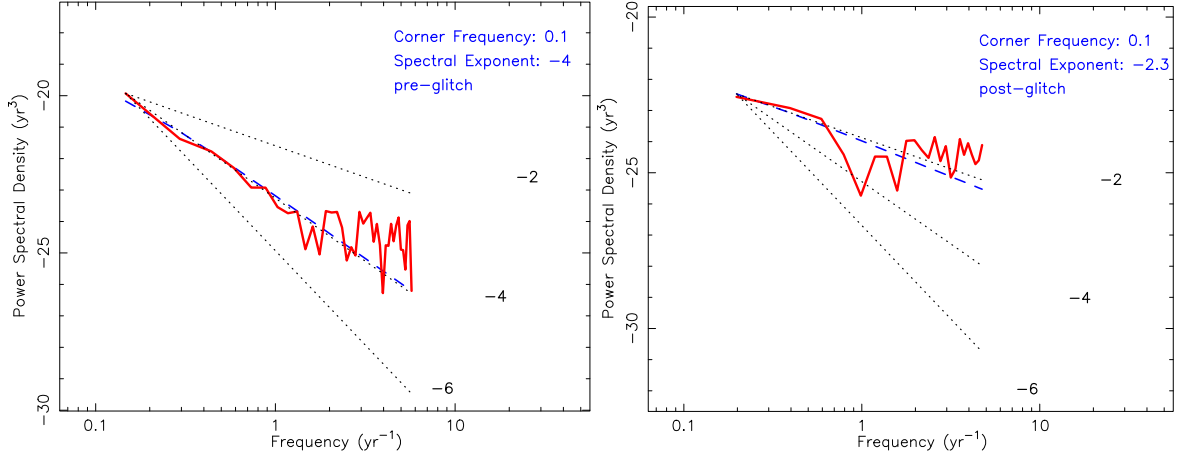


Figure 2. Power spectrum of the timing noise in PSR J1453–6413 before and after the second glitch. Left: Power spectrum of the pre-glitch timing noise. Right: Power spectrum of the post-glitch timing noise. The red solid lines are the observed spectral noise. The blue dashed lines in each panel represent the red noise model, and the dotted lines stand for the power spectrum with an exponent of -2 , -4 , and -6 from top to bottom, respectively.

We reconfirmed that the epoch of the first glitch is MJD 54554 (10), which is consistent with the previously reported epoch MJD 54552(4). The relative changes in spin frequency and spin-down rate of the first glitch are $1.9(4) \times 10^{-9}$ and $0.3(2) \times 10^{-3}$ respectively, which are smaller than the previously reported values $0.299(18) \times 10^{-9}$ and $0.55(11) \times 10^{-3}$, which may be because the previous study did not take the exponential recovery after this glitch into account. The results of our timing analysis show that the epochs for the second and third glitch are MJD 57093(18) and 59060(12) respectively. The relative changes of spin frequency and spin-down rate of the second glitch are $0.208(3) \times 10^{-9}$ and $0.035(3) \times 10^{-3}$, respectively. The relative changes in spin frequency and spin-down rate of the third glitch are $1.180(7) \times 10^{-9}$ and $0.50(2) \times 10^{-3}$ respectively. Obviously, the first glitch is the largest known glitch in PSR J1453–6413. However, it should be noted here that we did not consider the exponential recovery behavior in the analysis of the third glitch, so we could not be completely sure of the relative size of this glitch. Our results may need to be revised if exponential recovery behavior exists.

In addition, we also analyzed the post-glitch behavior of three glitches. The result shows that after the first glitch, the pulsar experienced an exponential recovery for about 200 days, with an exponential recovery factor $Q \approx 0.15(2)$. After the second glitch, it shows a linear recovery process. It should be noted that due to the lack of data after the third glitch, we are unable to analyze the post-glitch behavior of the third glitch. With the opening of the subsequent data, we will do further research on the post-glitch behavior of this glitch.

3.4. Timing noise

Coles et al. (2011) developed a method of determining pulsar timing solution by applying the ‘‘Cholesky’’ decomposition on

the covariance matrix of timing residual, which is an optimal technique to characterize strong red noise. Since PSR J1453–6413 has three glitches within the data span, we divided the data into four sections according to the epoch of glitches. However, because the data span of the first and last sections is insufficient, we only analyzed the timing noise power spectrum of the data span before and after the second glitch (see: Figure 2). The power spectrum can be modeled by a power law $P(f) = A/[1 + (f/f_c)^2]^{\alpha/2}$, where A , f_c , and α represent amplitude, corner frequency, and spectral index, respectively (Coles et al. 2011). The dotted lines in Figure 2 indicate the spectral exponent of -2 , -4 , and -6 , which suggest that the noise is dominated by a random walk in the phase, ν , and $\dot{\nu}$, respectively (Boynton et al. 1972). For the pre-glitch data, a mode with $\alpha = -4$ and $f_c = 0.1 \text{ yr}^{-1}$ could nicely describe the power spectrum of the timing noise. And for the post-glitch data, these values are $\alpha = -2.3$ and $f_c = 0.1 \text{ yr}^{-1}$ for a reasonable fit. These results show that the red noise before the second glitch is dominated by random walk in ν , while the red noise after this glitch the spectral index of which is close to -2 may be dominated by random walk in the phase. Our results indicate that the red noise of the pre-glitch data span may be dominated by the random walk in ν , while the red noise of the post-glitch data span may be dominated by random walk in the phase.

3.5. Correlation between Pulse Profile Changes and Glitches

In order to see if there is a correlation between glitches and profiles in PSR J1453–6413, we divided the data into four sections according to the epoch of three glitches and obtained the normalized mean pulse profiles before and after each glitch. It should be noted that due to the evolution of pulse profiles at

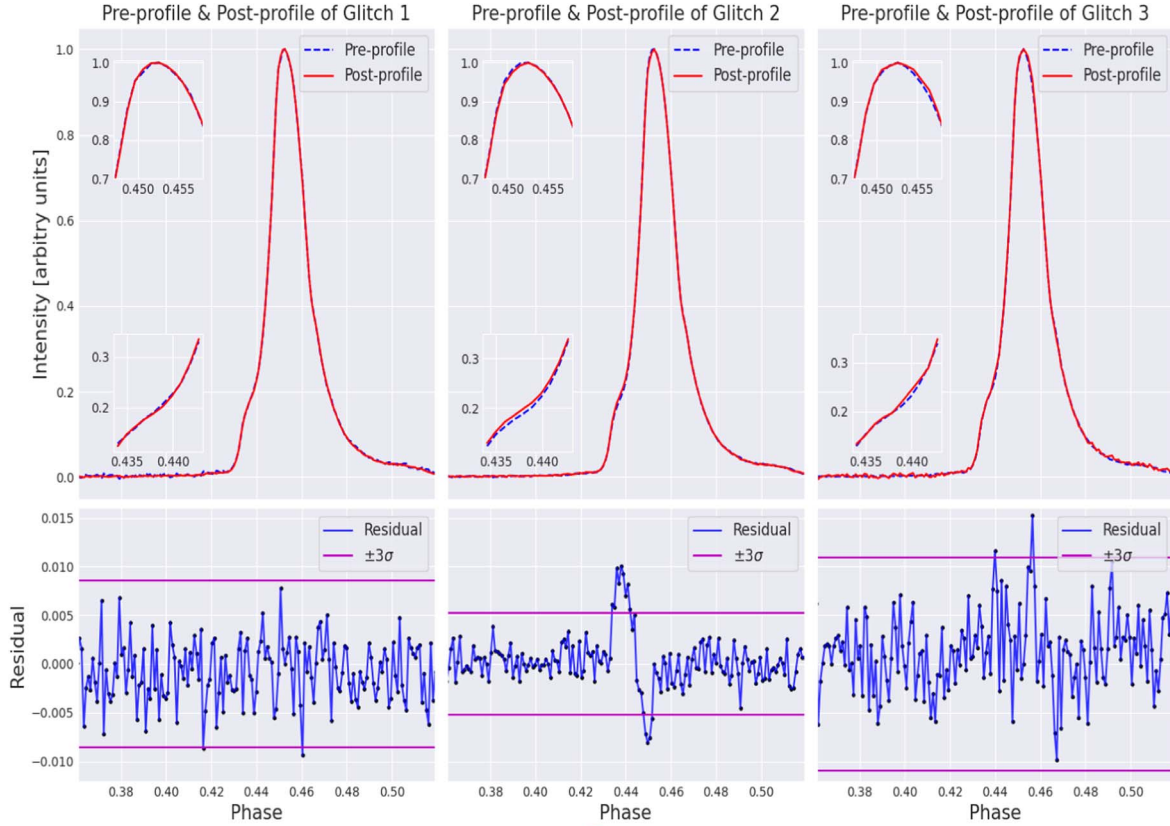


Figure 3. The pulse profile change around three glitches. In the top three panels, the blue dotted lines represent the normalized pulse profile before the glitch, the red solid lines represent the normalized pulse profile after the glitch. The inserts in each panel are the extent of pulse profiles near the 20% height of the pulse peak and the extent near the pulse peak. The bottom three panels show the residual of the pre- and post-glitch profiles. The purple solid lines in the three bottom panels represent the 3 times the maximum root mean square value of the profile residuals before and after the glitch.

different frequencies, the normalized mean pulse profile before the first glitch does not contain the data with a center frequency of 1374 MHz. Figure 3 shows the pulse profile change around three glitches. In the top three panels, the blue dotted lines represent the normalized pulse profiles before the glitch, the red solid lines represent the normalized pulse profiles after the glitch. The inserts in each panel are the extent of pulse profiles near the 20% height of the pulse peak and the extent near the pulse peak. The bottom three panels show the residual of the pre- and post-glitch profiles. The purple solid lines in the three bottom panels represent the 3 times the root mean square value of the profile residuals before and after the glitch. Obviously, there was no significant change in the integral pulse profiles before and after the first and third glitches, while there was a significant change in the pulse profiles before and after the second glitch, with the residual of the leading part and the residual at the peak significantly exceeding three times of its root mean square value. The leading component became stronger and the main component became weaker after the second glitch. Alternatively, the pulse profile widened near the

height of 20% of the pulse peak, but narrowed in front of the peak after the second glitch. However, due to the lack of data after the third glitch, we could not completely determine the correlation between the third glitch and the pulse profile change. With the release of subsequent data, we will further study the correlations between the glitch and the pulse profile change of PSR J1453–6413.

4. Discussion

4.1. Proper Motion

Pulsars are fast-moving objects whose space velocities are an order of magnitude larger than those of their progenitors (Gunn & Ostriker 1970; Hobbs et al. 2005). A natural explanation for such high velocities is that this is the result of a moment kick at birth (Lai & Qian 1998; Lai et al. 2001; Ng & Romani 2006). Velocities of pulsars are determined by measuring their proper motion and distance D . For high-intensity radio pulsars, Very Long Baseline Interferometry (VLBI) can be used to obtain their location and proper motion (Brisken et al. 2002, 2003; Deller et al. 2016). In recent years, VLBI has also obtained the

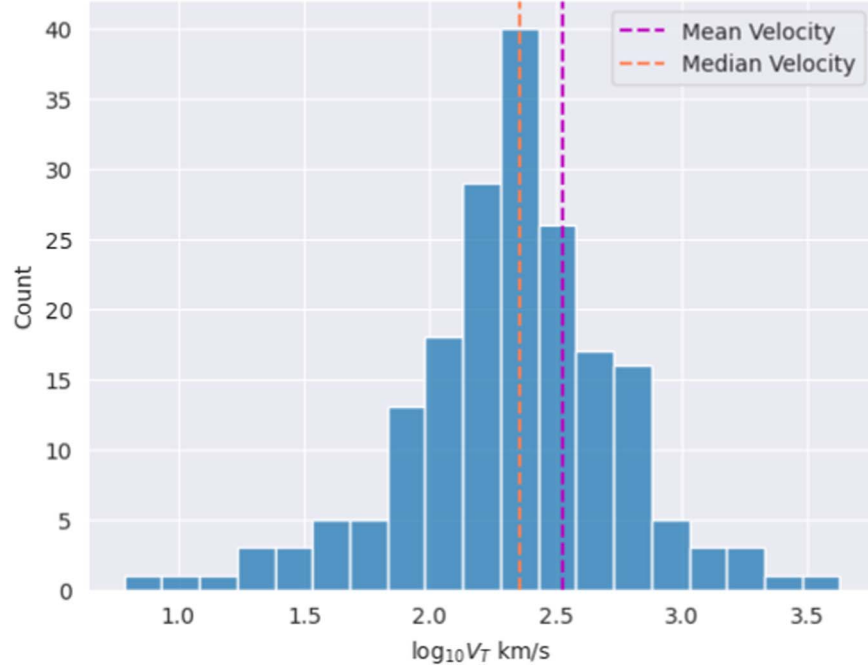


Figure 4. Distribution of the 2D transverse velocity. The longitudinal axis is the count. The horizontal axis is $\log_{10} V_T$, and the unit is km/s. The two vertical lines with different colors represent the median velocity and mean velocity, respectively.

proper motion of some weak pulsars, for example, Yan et al. (2013) used Very Long Base Array (VLBA) and European VLBI Network (EVN) to measure astrometric parameters of PSR B1257+12 in a three-planet pulsar system, and Du et al. (Du et al. (2014)) used EVN to obtain parallax and proper motion of weak millisecond pulsar PSR J0218+4232 at 1.6GHz. In addition, astrometric parameters can be determined by timing observations of pulsars spanning several years (Manchester et al. 1974; Hobbs et al. 2005; Li et al. 2016; Dang et al. 2020). In this paper, the position and proper motion of PSR J1453–6413 before and after the second glitch were obtained by using pulsar timing analysis. Although the accuracy of our results is not as high as that of the references due to the influence of red noise and the proper motion parameters being different before and after the second glitch, they are consistent within the error range.

The 2D transverse velocities of PSR J1453–6413 before and after the second glitch are $186(431) \text{ km s}^{-1}$ and $221(278) \text{ km s}^{-1}$, respectively. In order to compare the 2D transverse velocities of other pulsars, we used the data from the ATNF pulsar catalog to count the 2D transverse velocities of normal single pulsars. In this sample including 191 pulsars, the rotation period P of these pulsars is larger than 0.01s, and pulsars in binary systems were excluded. First, we used the distances which are best estimates using the YMW16 DM-based distance as default to count the velocities. Figure 4 shows that 2D transverse velocities of normal single pulsars in our sample are unimodal, the mean 2D transverse

velocity is $335(38) \text{ km}^{-1}$, and the median 2D transverse velocity is 229 km s^{-1} . In addition, the highest 2D speed in our sample is $4250(3607) \text{ km s}^{-1}$ for PSR J1829–1751, and the lowest 2D speed is $6(5) \text{ km s}^{-1}$ for PSR J1752–2806. Compare with our statistical result, the 2D transverse velocities of PSR J1453–6413 before and after the second glitch are consistent with the mean value within the margins of errors.

Moreover, Hobbs et al. (2005) counted the proper motion of 233 pulsars. Their results show that the mean 2D transverse velocities of normal single pulsars are $211(18) \text{ km s}^{-1}$ with the CL02 model (Cordes & Lazio 2002) and $269(25) \text{ km s}^{-1}$ with the TC93 model (Taylor & Cordes 1993). Inspired by them, we carried out simple statistics on the 2D transverse velocities of normal single pulsars, but the distances of these pulsars are all based on the YMW16 model. Our result in Figure 5 shows that the 2D transverse velocities of normal single pulsars based on the YMW16 model are also unimodal, the mean value is $395(44) \text{ km s}^{-1}$, the median value is 213 km s^{-1} , the highest speed is $5035(596) \text{ km s}^{-1}$ for PSR J2346–0609, and the lowest speed is $7(9) \text{ km s}^{-1}$. The difference in average two-dimensional transverse velocities between these two types may mainly come from the differences in the electron density models of the Galactic.

4.2. Glitch

We detected three glitches in PSR J1453–6413 using Parkes 64m radio telescope. The last two glitches are newly

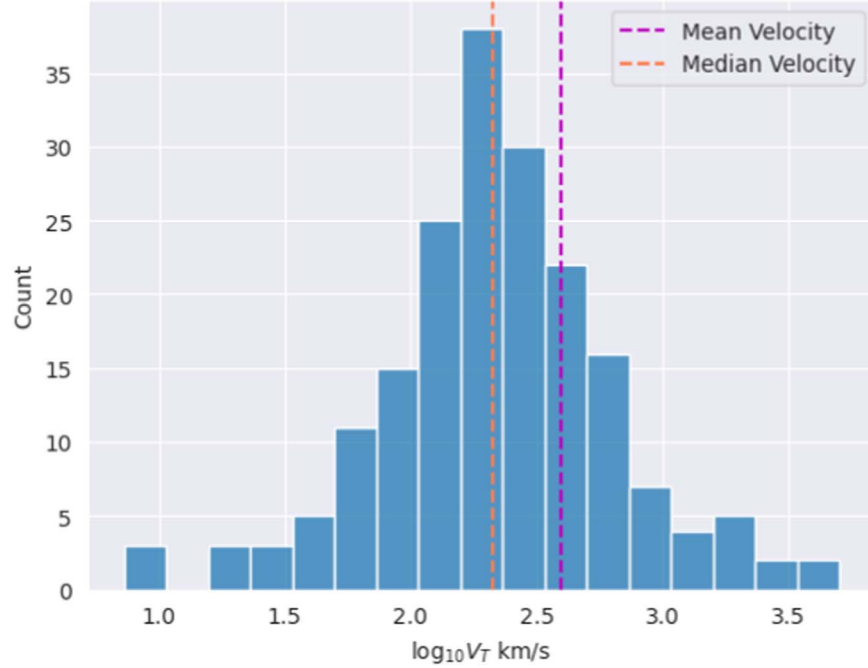


Figure 5. Distribution of the 2D transverse velocity based on the YMW16 model. The longitudinal axis is the count. The horizontal axis is $\log_{10} V_T$, and the unit is km/s. The two vertical lines with different colors represent the median velocity and mean velocity, respectively.

discovered in this study. These three glitches are all very small, which respectively have fractional sizes of $1.9(4) \times 10^{-9}$, $0.208(3) \times 10^{-9}$ and $1.180(7) \times 10^{-9}$. In the framework of the vortex model, the layer between the rapidly rotating superfluid and the shell leads to the Magnus force of crustal stress. When this force exceeds a critical threshold, the vortex will suddenly stop fixing. As a result, angular momentum is transferred to the crust causing a glitch.

If we assume that this pulsar star has only had three glitches, then we can obtain its glitch activity parameter, which is defined as

$$A_g = \frac{1}{T} \sum \frac{\Delta \nu_g}{\nu}, \quad (3)$$

where T is the total data span (McKenna & Lyne 1990; Lyne et al. 2000). For PSR J1453–6413, the corresponding value of $A_g \approx 1.41 \times 10^{-10} \text{ yr}^{-1}$. This is consistent with the assumption that the low glitch activity A_g of pulsars with small spin-down rate is caused by small and rare glitches (Lyne et al. 2000; Hobbs et al. 2010; Yuan et al. 2010b; Espinoza et al. 2011). Espinoza et al. (2011) reported a correlation between the mean glitch rate and spin-down rate with $\langle N_g \rangle \propto |\dot{\nu}|^{0.47(4)}$. This result suggests that pulsars with low spin-down rates tend to exhibit small glitches. It should be noted that this correlation is based on a large sample, those pulsars that did not be detected with glitches were included and some newly detected glitches were not included. For PSR J1453–6413 with

$|\dot{\nu}| \approx 85.1812 \times 10^{-15} \text{ s}^{-2}$, the predict $\langle N_g \rangle$ is in the range of $0.027(5)$ to $0.04(1) \text{ yr}^{-1}$. The observed mean glitch rate is large with the value of $\approx 0.13 \text{ yr}^{-1}$, which is about 3.3 to 4.8 times that of the predicted value. This suggests that, in terms of glitch, PSR J1453–6413 is more active than those with similar spin-down rates.

We investigated radio Pulsar with characteristic ages between 1.0×10^6 and $1.5 \times 10^6 \text{ yr}$, and found that only 11 pulsars were detected to have undergone glitches, with a total glitch number of 30.^{13,14} These pulsars including PSR J1453–6413, and six pulsars (PSRs J0528+2200, J1453–6413, J1705–1906, J2225+6535, J1812–1718) have each at least three glitches observed (Backus et al. 1982; Janssen & Stappers 2006; Yuan et al. 2010b; Espinoza et al. 2011; Yu et al. 2013; Liu et al. 2018; Basu et al. 2022). For those radio pulsars with similar period P (from 0.17 s to 0.19 s) and similar \dot{P} (from 1×10^{-14} to 1×10^{-13}), no glitch was observed expected PSR J1453–6413. Almost all glitches of these pulsars with similar characteristic ages and spin parameters have relative sizes of $\approx 10^{-9}$, except for the glitches in PSRs J0611+1436 and J2225+6535, which have relative glitch sizes of $\approx 10^{-6}$ (Backus et al. 1982; Basu et al. 2022). Therefore, we could not rule out the possibility of large glitches happening to PSR J1453–6413.

¹³ <https://www.atnf.csiro.au/people/pulsar/psrcat/glitchTbl.html>

¹⁴ <https://www.jb.man.ac.uk/pulsar/glitches/gTable.html>

There are two popular theories to explain the glitches of pulsars. The first theory holds that the glitch is caused by starquakes, and the second theory holds that the glitch is caused by the interaction between the superfluid inside the pulsar and the solid crust. The former can only explain the glitch of a few pulsars (Ruderman 1991; Ruderman et al. 1998), while the latter is the mainstream theory at present, which can be used to explain the glitch of most pulsars (Anderson & Itoh 1975; Piekarewicz et al. 2014). The coupling parameters between the superfluid inside the pulsar and the outer crust are defined as $G = \tau_c A_g = \frac{v-1}{|\dot{\nu}|T} \sum \frac{\Delta\nu_g}{\nu}$. Here $\frac{I_c}{I} \geq G$, I_c is the moment of inertia of the crust superfluid and I is the total moment of inertia. For Vela-like mature pulsars which glitch frequently and experience large glitches, if we consider the exit of the crustal entrainment, the lower limit of $\frac{I_c}{I}$ is 1.6% ~ 7% (Piekarewicz et al. 2014). More than 7% will result in the superfluid in the crust cannot meet the angular momentum required by the glitch, and other possibilities such as core superfluid involvements should be considered (Ho et al. 2015). For PSR J1453–6413, the corresponding $\frac{I_c}{I}$ is about 0.029%, which lies within the theoretical expectations of superfluid theories (Piekarewicz et al. 2014). Its small value of $\frac{I_c}{I}$ could result from the non-detection of large glitches in PSR J1453–6413 during our current observational time span. In other words, if another glitch of magnitude 10^{-8} should be found in the future, the fractional moment of inertia $\frac{I_c}{I}$ will increase by one order of magnitude and return to normal.

4.3. Correlation between Pulse Profile Changes and Glitches

Increasing evidence shows that there seem to be some complex correlations between pulsars spin and emission. However, we could not fully understand these correlations at present. Nevertheless, the view that the measurable changes in spin-down rate, flux, and pulse shape of pulsars are driven by a shift in the magnetic inclination angle α as a consequence of a glitch, has gradually become a consensus (Link & Epstein 1997; Akbal et al. 2015; Ng et al. 2016; Liu et al. 2021). In general, the glitch is thought to originate inside the neutron star, but the emission is thought to originate in the magnetosphere of the neutron star. The phenomenon of emission changed by glitches has provided an opportunity for us to study the interaction between spin and emission. The change of $\Delta\dot{\nu}$ reflects the change of external braking torque of the pulsar. The permanent relative change of $\Delta\dot{\nu}$ can be caused by change in inclination angle (Link et al. 1992; Link & Epstein 1997). According the MHD simulation of Spitkovsky (Spitkovsky (2006)), the relationship between the magnetic angle α and change of spin-down rate $\Delta\dot{\nu}/\dot{\nu}$ can be expressed as follows: $\frac{\sin 2\alpha\Delta\alpha}{(1+\sin^2\alpha)^2}$. Glitch may lead to the change of the pulsar magnetic field structure and the inclination angle (Ng et al. 2016).

Corresponding to the increase of 0.0035% in $\Delta\dot{\nu}/\dot{\nu}$ of PSR J1453–6413, the expected change in inclination angle is $\Delta\alpha \approx 0^\circ.003$, if we assume the inclination angle for this pulsar is 45° . The change in inclination angle will cause the change of effective emission geometry, which will result in the change of pulse profile we observed. Here we can see that change in the inclination angle of this pulsar is very small, which is consistent with the small change in the pulse profile we observed.

5. Summary

We have presented a timing analysis of PSR J1453–6413 based on 23.3 yr of observations using the Parkes 64-m radio telescope. The main conclusions are as follows:

1. Using the Colesky method, we obtained the improved values of position, proper motion, velocity, and spin parameters of this pulsar.
2. We confirmed the first glitch of this pulsar in MJD 54554 (10) and detected an exponential recovery of this glitch, with a timescale of about 200 days and the corresponding Q factor is about 0.15. Besides, we also detected two new glitches that occurred in MJD 57093(18) and 59060(12), respectively. The relative sizes of these three glitches are $1.9(4) \times 10^{-9}$, $0.208(3) \times 10^{-9}$ and $1.180(7) \times 10^{-9}$, respectively.
3. We obtained the power spectrum of the timing noise of this pulsar, and found that the red noise before the second glitch may be dominated by the random walk in ν , while the red noise after the second glitch may be dominated by the random walk in the pulse phase.
4. We detected the glitch correlated profile changing of the second glitch. The leading component of the integral pulse profile after the second glitch became stronger, while the main component became weaker.

We look forward to collecting more observations in the future to further investigate the correlation between the glitches and pulse profile changes of PSR J1453–6413.

Acknowledgments

This work was supported by the National SKA Program of China (Nos. 2022SKA0130100, 2020SKA0120100 and 2022SKA0130104), Guizhou Province Science and Technology Foundation (No. ZK[2022]304), the Major Science and Technology Program of Xinjiang Uygur Autonomous Region (Nos. 2022A03013-2 and 2022A03013-4), the Scientific Research Project of the Guizhou Provincial Education (Nos. KY[2022]132, KY[2022]123 and KY[2022]137), the National Natural Science Foundation of China (Nos. 11873080, U1731238, 11565010, 12103013, U1838109, U1831120, 12273008 and 12103013), the Joint Research Fund in Astronomy under cooperative agreement between the National

Natural Science Foundation of China and Chinese Academy of Sciences (No. U1931101), the Foundation of Guizhou Provincial Education Department (Nos. KY(2020)003 and KY(2021)303), the Guizhou Province Science and Technology Support Program (No. [2023] General 333), the 2021 project Xinjiang Uygur autonomous region of China for Tianshan elites, the Key Laboratory of Xinjiang Uygur Autonomous Region No. 2020D04049, the Academic New Seeding Fund Project of Guizhou Normal University (No. [2022]B18) and the CAS Jianzhijia project. The Parkes radio telescope is part of the Australia Telescope National Facility which is funded by the Commonwealth of Australia for operation as a National Facility managed by CSIRO. This paper includes archived data obtained through the CSIRO Data Access Portal.

ORCID iDs

Wei Li  <https://orcid.org/0009-0009-8247-3576>

Shi-Jun Dang  <https://orcid.org/0000-0002-2060-5539>

References

- Akbal, O., Gügerçinoğlu, E., Şaşmaz Muş, S., & Alpar, M. A. 2015, *MNRAS*, **449**, 933
- Anderson, P. W., & Itoh, N. 1975, *Natur*, **256**, 25
- Backus, P. R., Taylor, J. H., & Damashek, M. 1982, *ApJL*, **255**, L63
- Bailes, M., Manchester, R. N., Kesteven, M. J., Norris, R. P., & Reynolds, J. E. 1990, *MNRAS*, **247**, 322
- Basu, A., Shaw, B., Antonopoulou, D., et al. 2022, *MNRAS*, **510**, 4049
- Boynton, P. E., Groth, E. J., Hutchinson, D. P., et al. 1972, *ApJ*, **175**, 217
- Brisken, W. F., Benson, J. M., Goss, W. M., & Thorsett, S. E. 2002, *ApJ*, **571**, 906
- Brisken, W. F., Fruchter, A. S., Goss, W. M., Herrnstein, R. M., & Thorsett, S. E. 2003, *AJ*, **126**, 3090
- Cheng, K. S. 1987a, *ApJ*, **321**, 805
- Cheng, K. S. 1987b, *ApJ*, **321**, 799
- Coles, W., Hobbs, G., Champion, D. J., Manchester, R. N., & Verbiest, J. P. W. 2011, *MNRAS*, **418**, 561
- Cordes, J. M., & Lazio, T. J. W. 2002, arXiv:astro-ph/0207156
- D'Alessandro, F. 1996, *Ap&SS*, **246**, 73
- Dang, S.-J., Wang, N., Wang, H.-H., et al. 2021, *RAA*, **21**, 042
- Dang, S. J., Yuan, J. P., Manchester, R. N., et al. 2020, *ApJ*, **896**, 140
- Deller, A. T., Vigeland, S. J., Kaplan, D. L., et al. 2016, *ApJ*, **828**, 8
- Deng, X. P., Hobbs, G., You, X. P., et al. 2013, *AdSpR*, **52**, 1602
- Du, Y., Yang, J., Campbell, R. M., et al. 2014, *ApJL*, **782**, L38
- Edwards, R. T., Hobbs, G. B., & Manchester, R. N. 2006, *MNRAS*, **372**, 1549
- Espinoza, C. M., Lyne, A. G., Stappers, B. W., & Kramer, M. 2011, *MNRAS*, **414**, 1679
- Gunn, J. E., & Ostriker, J. P. 1970, *ApJ*, **160**, 979
- Ho, W. C. G., Espinoza, C. M., Antonopoulou, D., & Andersson, N. 2015, *SciA*, **1**, e1500578
- Hobbs, G., Lorimer, D. R., Lyne, A. G., & Kramer, M. 2005, *MNRAS*, **360**, 974
- Hobbs, G., Lyne, A. G., & Kramer, M. 2010, *MNRAS*, **402**, 1027
- Hobbs, G., Lyne, A. G., Kramer, M., Martin, C. E., & Jordan, C. 2004, *MNRAS*, **353**, 1311
- Hobbs, G., Miller, D., Manchester, R. N., et al. 2011, *PASA*, **28**, 202
- Hobbs, G. B., Edwards, R. T., & Manchester, R. N. 2006, *MNRAS*, **369**, 655
- Hotan, A. W., van Straten, W., & Manchester, R. N. 2004, *PASA*, **21**, 302
- Janssen, G. H., & Stappers, B. W. 2006, *A&A*, **457**, 611
- Jones, P. B. 1990, *MNRAS*, **246**, 364
- Keith, M. J., Shannon, R. M., & Johnston, S. 2013, *MNRAS*, **432**, 3080
- Kou, F. F., Yuan, J. P., Wang, N., Yan, W. M., & Dang, S. J. 2018, *MNRAS*, **478**, L24
- Kramer, M., Stairs, I. H., Manchester, R. N., et al. 2006, *Sci*, **314**, 97
- Lai, D., Chernoff, D. F., & Cordes, J. M. 2001, *ApJ*, **549**, 1111
- Lai, D., & Qian, Y.-Z. 1998, *ApJ*, **505**, 844
- Li, L., Wang, N., Yuan, J. P., et al. 2016, *MNRAS*, **460**, 4011
- Link, B., & Epstein, R. I. 1997, *ApJL*, **478**, L91
- Link, B., Epstein, R. I., & Baym, G. 1992, *ApJL*, **390**, L21
- Liu, J., Wang, H.-G., Shen, Z.-Q., et al. 2022, *ApJ*, **931**, 103
- Liu, J., Wang, H.-G., Yan, Z., et al. 2021, *ApJ*, **912**, 58
- Liu, Y., Xu, B., Zheng, Z., Chen, Z., & Zhu, X. 2023, *MNRAS*, **521**, 2553
- Liu, Y. L., Yuan, J. P., Wang, J. B., et al. 2018, *Ap&SS*, **363**, 96
- Lyne, A. G., Shemar, S. L., & Smith, F. G. 2000, *MNRAS*, **315**, 534
- Manchester, R. N., Hobbs, G. B., Teoh, A., & Hobbs, M. 2005, *AJ*, **129**, 1993
- Manchester, R. N., Taylor, J. H., & Van, Y. Y. 1974, *ApJL*, **189**, L119
- McKenna, J., & Lyne, A. G. 1990, *Natur*, **343**, 349
- Melatos, A., & Link, B. 2014, *MNRAS*, **437**, 21
- Ng, C. W., Takata, J., & Cheng, K. S. 2016, *ApJ*, **825**, 18
- Ng, C. Y., & Romani, R. W. 2006, *ApJ*, **644**, 445
- Palfreyman, J., Dickey, J. M., Hotan, A., Ellingsen, S., & van Straten, W. 2018, *Natur*, **556**, 219
- Parthasarathy, A., Shannon, R. M., Johnston, S., et al. 2019, *MNRAS*, **489**, 3810
- Piekarewicz, J., Fattoyev, F. J., & Horowitz, C. J. 2014, *PhRvC*, **90**, 015803
- Ruderman, M. 1976, *ApJ*, **203**, 213
- Ruderman, M. 1991, *ApJ*, **382**, 587
- Ruderman, M., Zhu, T., & Chen, K. 1998, *ApJ*, **492**, 267
- Spitkovsky, A. 2006, *ApJL*, **648**, L51
- Taylor, J. H., & Cordes, J. M. 1993, *ApJ*, **411**, 674
- Weltervrede, P., Johnston, S., & Espinoza, C. M. 2011, *MNRAS*, **411**, 1917
- Yan, Z., Shen, Z.-Q., Yuan, J.-P., et al. 2013, *MNRAS*, **433**, 162
- Yao, J. M., Manchester, R. N., & Wang, N. 2017, *ApJ*, **835**, 29
- Yu, M., Manchester, R. N., Hobbs, G., et al. 2013, *MNRAS*, **429**, 688
- Yuan, J. P., Manchester, R. N., Wang, N., et al. 2010a, *ApJL*, **719**, L111
- Yuan, J. P., Wang, N., Manchester, R. N., & Liu, Z. Y. 2010b, *MNRAS*, **404**, 289
- Zhou, S. Q., Gügerçinoğlu, E., Yuan, J. P., et al. 2023, *MNRAS*, **519**, 74